Single-electrolyte isotachophoresis : on-chip analyte focusing and separation

Quist, J.W.

5 PDMS Valves as Tunable Nanochannels for Concentration Polarization

Published in Lab on a Chip 2013, 13, pp 4810-4815

Elastomeric microvalves in poly(dimethylsiloxane) (PDMS) devices are today's paradigm for massively parallel microfluidic operations. Here we report that such valves can act as nanochannels upon closure. When tuning nanospace heights between ~55 nm and ~7 nm, the nanofluidic phenomenon of concentration polarization could be induced. A wide range of concentration polarization regimes (anodic and cathodic analyte focusing and stacking) was achieved simply by valve pressure actuation. Electro-osmotic flow generated a counterpressure, therefore voltage actuation also could be used to actuate between concentration polarization regimes. 1000-fold preconcentration of fluorescein was achieved in just 100 s in the anodic focusing regime. After valve opening, a concentrated sample plug could be transported through the valve, though at the cost of some defocusing. Reversible nanochannels open new avenues for integrating electrokinetic operations and assays in large scale integrated microfluidics.

During the last decade, many applications have been developed for microfluidic devices with integrated nanofluidic components[1]. One important property of nanofluidic components is perm-selectivity. Perm-selectivity results from the dominance of surface charge inside nanofluidic conducts, excluding co-ions and enriching counterions[2, 3]. This has led to the development of fluidic diodes[4, 5] and transistors[6]. An important accompanying

effect is concentration polarization: upon application of a voltage potential, ion enrichment and ion depletion zones arise at each entrance of the nanofluidic conduit respectively[7, 8]. In the case of a negative surface charge, for example in materials like glass, silicon and poly(dimethylsiloxane) (PDMS), a depletion zone is formed at the anodic entrance of the nanofluidic conduct. The sharp conductivity gradient at the border of the ion-depleted zone can be used for very efficient preconcentration of charged analytes ranging from proteins to nucleic acids and metabolites[9, 10]. Concentration factors exceeding a million have been reported[9, 11]. Based on this effect, we recently reported depletion zone isotachophoresis (dzITP), a simple and versatile method for focusing, separation and positioning of analytes[12, 13] (chapter 3 and 4). These effects have been employed in immuno- and enzyme assays[10, 14]. Other applications of on-chip concentration polarization include rapid mixing by electrokinetic instabilities of the depletion zone[15] and seawater desalination[16].

In a theoretical study of analyte preconcentration in micro-nano-micro structures, Plecis et al[17] have identified four different concentration polarization regimes. The four regimes correspond to the four interfaces where the balance between bulk flow (EOF) versus electrophoretic transport of analytes changes. In order of increasing bulk flow, cathodic stacking (CS) occurs at the cathodic entrance of a nanopore; cathodic counter gradient focusing (CCGF) occurs at the border of the enrichment zone; anodic counter gradient focusing (ACGF) occurs at the border of the depletion zone and anodic stacking (AS) occurs at the anodic entrance of the nanochannel. The model indicated that the ACGF regime is most efficient for analyte preconcentration. This must be explained by the facts that I) the stacking regimes allow for analyte leakage through the nanochannel, while in the

focusing regimes all analytes are trapped; and II) the depletion zone interface has a much sharper electric field gradient than the enrichment zone interface. The ACGF regime and variants thereof are indeed very common in concentration polarization-based preconcentration devices.

To our knowledge, in literature no description can yet be found of a device that is able to reach all four concentration polarization regimes. We here propose to use elastomeric microvalves for tuning nanochannels to achieve various concentration polarization regimes. Such elastomeric microvalves are one of the most important and well-known inventions in the field of microfluidics, because they are easy to implement and offer the possibility to create large-scale integrated fluidic networks[18]. An elastomeric microvalve consists of a membrane between a fluidic channel and a control channel. When the control channel is pressurized, the membrane will deflect, displacing the fluid and closing off the fluidic channel[19]. Under certain conditions, upon closing the microvalve a nanometer-sized fluidic layer remains between the membrane and the wall of the fluidic channel. Because at sufficiently high pH's PDMS has a negative surface charge this effectively creates a perm-selective nanochannel. Kuo et al used this effect for a normally closed PDMS valve to trap DNA that upon opening could be released [23].

In this paper we use elastomeric microvalves to create reversible and tunable nanospaces. Measurements of electrical resistance at different valve pressures indicate that in addition to full open or closure, nanospace height can be varied between ~55 nm and ~7 nm. Different concentration polarization regimes could be obtained by variation of the valve pressure and corresponding nanospace dimensions. Variation of voltages results in changes in electro-osmotic flow (EOF)-induced counterpressure, which also leads to

different concentration polarization regimes. Co-optimization of valve pressure and voltage resulted in a very efficient ACGF regime, by which a 1000-fold preconcentration of fluorescein was achieved in just 100 seconds. Preconcentrated sample could be released by opening the valve. Tunable PDMS nanochannels offer increased control over polarisation concentration phenomena that can be seamlessly integrated in large scale integrated microfluidics.

Experimental

Chemicals.

Lithium carbonate was obtained from Acros Organics (Geel, Belgium), disodium fluorescein was obtained from Riedel-de Haen (Seelze, Germany). Before each experimental series, solutions were prepared fresh from stock solutions.

Device fabrication and preparation.

Chips were fabricated using well established multilayer soft lithography methods[19, 20]. Briefly, fluidic and pneumatic masters were fabricated by spin coating a 13µm film of ma-P 1275 (MicroResist Technology GmbH, Berlin, Germany) on glass substrates (Berliner Glas KGAA, Berlin, Germany) and prebaking for 2 minutes at 65˚C, 115˚C and 65˚C consecutively. After exposure using a Karl Suss MA45 mask aligner (SÜSS MicroTec AG, Garching, Germany) and development with MAD 332 developer (MicroResist Technology GmbH, Berlin, Germany). To ensure rounded channels, wafers were reflow baked on a controlled hotplate by ramping to 114 ˚C in 15 minutes and baking for 20 min. Polydimethylsiloxane (Sylgard 184, Dow Corning,

Midland, MI) base and curing agents were mixed 10:1 (w:w), degassed and cast on masters and cured. PDMS membranes were prepared by spincoating the same PDMS on a glass substrate (2300 rpm, 75 s) and curing. After dicing and punching of access holes, the fluidic structures and membrane were bonded after oxygen plasma treatment(Femto Plasma System, Diener, Ebhausen, Germany) and bonded. Pneumatic structures containing the control channels were bonded to the other side of the membrane using the same process. The fluidic channels had 160.7 ± 3.1 μm width and 13.4 ± 0.9 μm height in the devices used for the resistance measurements. The control channel width (and therefore the unclosed valve membrane width) was 133.3 ± 2.7 μm. For the devices used in the concentration polarization experiments, the fluidic channel had 108.5 ± 2.7 μm width.

For channel filling, solutions were injected into the channels using a syringe. The control channel was dead-end filled with deionized water in order to prevent bubble formation caused by gas permeation through the valve membrane. The fluidic channel was flushed electrokinetically between concentration polarization experiments with identical solutions.

Setup and Microscopy

For voltage actuation, an ES 0300 045 power supply (Delta Elektronika BV, Zierikzee, The Netherlands) was used, which was controlled by an NI USB 6221 data acquisition system using LabVIEW 8.2 software (National Instruments, Austin, TX). Currents were amplified using a Keithley 427 current amplifier (Keithley Instruments, Cleveland, OH) and were recorded using the NI USB 6221 device and LabVIEW. For current actuation, a Keithley 2410 sourcemeter unit was used. Microvalve pressure was regulated using a

Camozzi MC104 reducing valve (Camozzi spa, Brescia, Italy). On/off switching of the pressure was done using a solenoid valve (Isonic V1, Mead Fluid Dynamics inc, Chicago, IL) Microscopy was performed with an Olympus IX71 microscope (Olympus, Zoeterwoude, The Netherlands) to which an Hamamatsu Orca-ER digital camera was mounted, which was controlled by Hokawo version 2.1 imaging software (Hamamatsu Photonics, Nuremberg, Germany). The magnification was 40x.

The effect of valve pressure (0.5-3.0 bar) on concentration polarization was investigated using 2.0 mmol/L lithium carbonate, pH 10.5 as the electrolyte. 40 µmol/L fluorescein was used as the analyte. A constant current of 100 µA was applied. The same electrolyte conditions were used in the constant voltage experiments, in these experiments 20 µmol/L fluorescein was used as the analyte; the valve pressure was 1.5 bar.

Data processing.

Charge coupled device (CCD) images were processed using the Hokawo version 2.1 software. All CCD images show a channel section with 2.1 mm length. Fluorescence intensity values were calculated in ImageJ (http://rsb.info.nih.gov/ij/) by averaging 20 image lines in the center of the fluidic channel and correcting for background signal.

Results

Reversible perm-selective nanospace concept.

Figure 1a depicts the concept of using a conventional elastomeric microvalve for concentration polarization purposes. The fluidic channel has a rounded

cross-section to allow uniform contact between the valve membrane and the channel wall upon pressurization of the control channel.

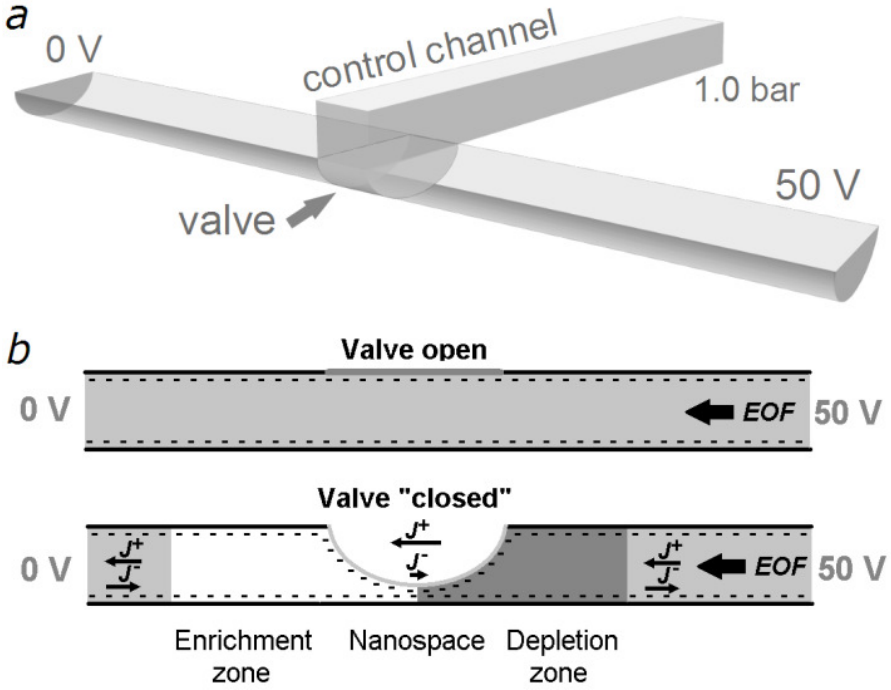

Figure 1. Schematic representations of the microvalve and the concentration polarization process with examples of applied voltages and pressures. a) 3d scheme of an elastomeric microvalve. The valve membrane is deflected by applying a pressure on the control channel. The fluidic channel is rounded to allow closure across the complete cross-section of the channel. b) Concentration polarization process across the nanospace which remains under the closed valve. J+ and J- represent cation and anion fluxes respectively; due to the imbalance of these fluxes depletion and enrichment zones are formed after valve closure. Schematic representations of the microvalve and the concentration polarization process with examples of applied voltages and pressures. a) 3d scheme of an elastomeric microvalve. The valve membrane is deflected by applying a pressure on the control channel. The fluidic channel is rounded to allow closure across the complete cross-section of the channel. b) Concentration polarization process across the nanospace which remains under the closed valve. J^+ and J^- represent cation and anion fluxes respectively; due to the imbalance of these fluxes depletion and enrichment zones are formed after valve closure.

Figure 1b shows how the surface charge of the PDMS (which results from deprotonation of SiOH groups) causes concentration polarization once a nanospace is formed upon partial closure of the valve. Negative surface charges on the PDMS surface are dominant in the nanospace, causing the current through the nanospace to be mostly carried by cations. Away from the nanospace, the fraction of the volume in the microchannel affected by the surface charge is too small to significantly achieve the same effect.
The resulting imbalance in anion and cation transport leads to the formation of an ion-depleted zone at the anodic side of the valve, while at the cathodic side an enrichment zone is formed. At the border of these zones, analytes can be focussed or stacked.

Nanospace tunability.
The size of the nanospace can be tuned by controlling the pressure applied to the control channel. The electrical resistance of the nanospace is estimated by measuring currents immediately before and after valve closure, while applying a constant voltage of 40V (figure 2). In this experiment, concentration polarization effects were suppressed through the use of a 100 mmol/L HCl electrolyte. Resistance values for channel with closed valve were corrected with the resistance of the open channel in order to obtain the valve resistance. Resistance values vary from 1.39 ± 0.20 MΩ at 0.5 bar to 46.13 ± 5.31 MΩ at 3.0 bar. We observed that the area of the valve where the membrane was contacting the opposite wall also depended on the pressure. The width of this "closed" surface varied from ~25 µm at 0.5 bar to ~85 µm at 3 bar. When taking into account the width and the resistance of the closed valve versus the length and the resistance of the fluidic channel, and assuming uniform valve

closure, the nanospace height can be roughly estimated. The resistivity of the closed valve was ~250x (at 0.5 bar) to ~2000x (at 3 bar) higher than the resistivity of the fluidic channel. This leads to a rough estimate for nanospace heights from 55 nm at 0.5 bar down to 7 nm at 3.0 bar.

In some previous studies[21, 22], much higher electrical resistances were reported. These values are expected to be strongly dependant on the device geometry including channel height, width and curvature, as well as membrane width, thickness and elasticity.

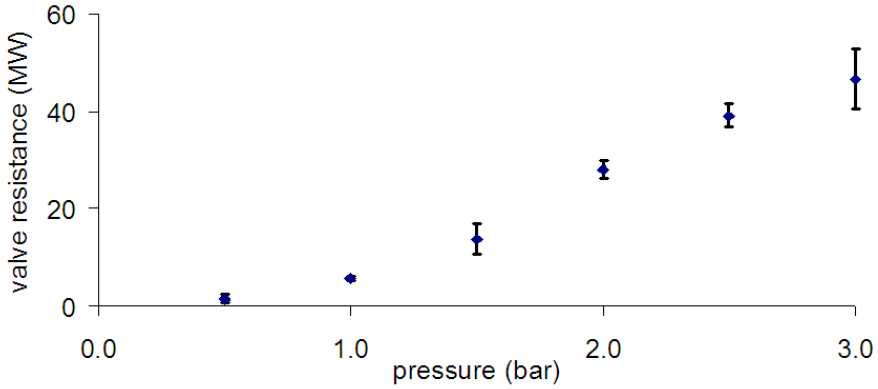

Figure 2. Graph of valve resistance versus valve pressure in a 100 mmol/L HCl solution. Measurements were triplicated and randomized.

Concentration polarization regimes through pressure-induced tunability.

Figure 3 shows a number of concentration polarization phenomena at various pressures that correlate to the different concentration polarization regimes described by Plecis et al.[17]. At 0.5 bar, the fluorescein was efficiently concentrated directly at the edge of the closed valve membrane. After ~35 seconds, however, more and more fluorescein leaked through the nanospace into the cathodic part of the channel, although concentration of fluorescein still occurred. This combination of analyte concentration and leakage through

a nanospace corresponds to the AS regime. At 1.0 and 1.5 bar, the ACGF regime was observed. In this regime the fluorescein focused most efficiently.

Figure 3. Concentration polarization regimes at different valve pressures in a 2.0 mmol/L lithium carbonate solution containing 40 µmol/L fluorescein. A constant current of 100 µ□A was applied. Images were taken 20 s after valve closure.

At 1.0 bar, a very small depletion zone was observed, which hardly grew. At 1.5 bar, a slowly growing depletion zone was present. At 2.0 bar, there is a transition between the ACGF and the CCGF regime. Some focusing takes place both at the cathodic and the anodic side, though very inefficient. From

2.0 bar and higher, a rapidly growing depletion zone was observed. At the edges of the channel, clearly some fluorescein remains. It appears that the EOF, encountering the closed valve as a hydrostatic barrier, generates a hydrodynamic counterflow which strongly promotes depletion zone growth in the middle of the channel. At the edges, the rounded fluidic channel is very shallow, suppressing the hydrodynamic counterflow and allowing the non-depleted liquid to stay. Due to this effect, large depletion zones will be disadvantageous for preconcentration purposes because sample dispersion may become very significant. At 2.5 and 3 bar, we observe CCGF regimes. Plecis et al.[17] distinguished between stable and unstable CCGF; in unstable CCGF the focused peak shifts position away from the nanochannel. Stable CCGF occurs at lower flow rates and has more efficient focusing. The regime observed at 2.5 bar is clearly a case of unstable CCGF, while the regime at 3 bar is more similar to stable CCGF, as the concentrated sample peak moved much slower away from the valve. A CS regime is expected to occur at even higher valve pressures. Such pressures would however compromise the structural integrity of the device and could thus not be tested. Nevertheless, CS was observed when applying a low voltage, as discussed in the next section.

The decrease in bulk flow due to increased hydraulic resistance is the most likely explanation of the observed differences in concentration polarization regimes.

By using different pressures for valve actuation, we have achieved at least three of the regimes described in the study of Plecis et al.[17], namely the CCGF, the ACGF and the AS regime. Increasing pressures decrease the the nanospace under the nearly closed valve, which leads to: I) greater perm-selectivity, resulting in stronger concentration polarization and II) decreased bulk flow,

because the nearly closed valve acts as a hydrostatic barrier which counters EOF.

Concentration polarization regimes at different voltages.

Figure 4 shows a range of concentration polarization regimes under varying applied voltages. At 20V, we observe a CS regime, with highest fluorescein concentrations directly at the cathodic side of the closed valve membrane.

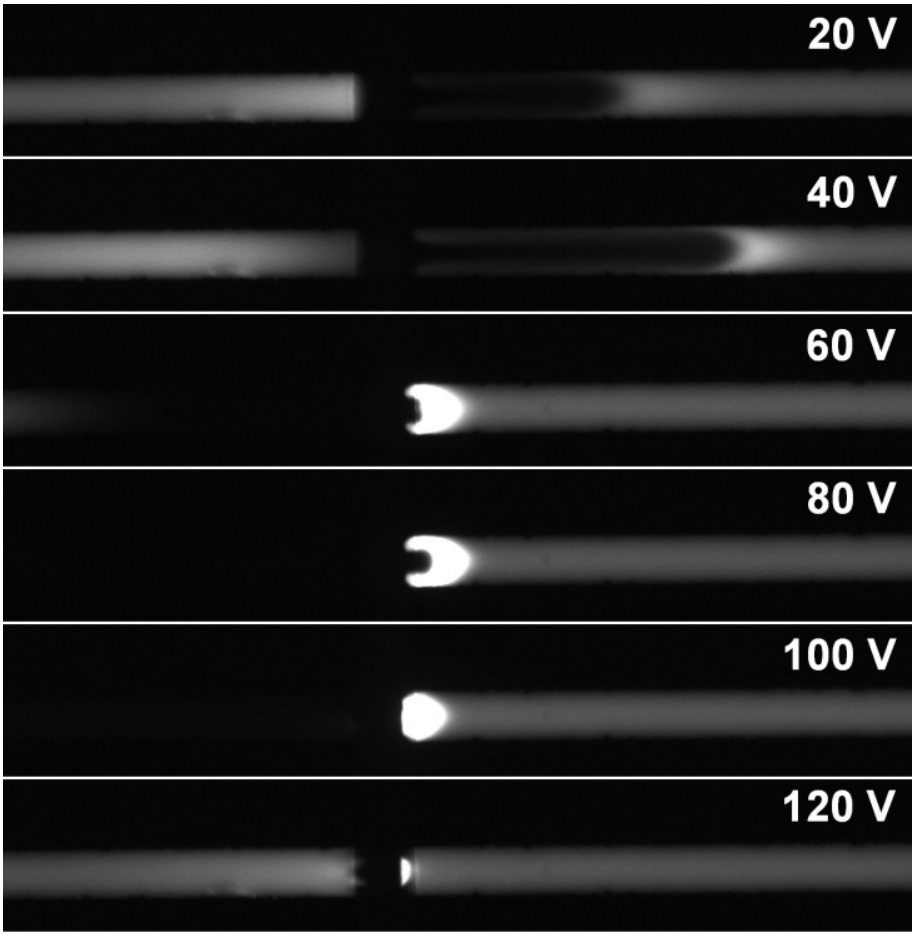

Figure 4. Concentration polarization regimes at different voltages in a 2 mmol/L lithium carbonate solution containing 20 µmol/L fluorescein. Valve pressure was 1.5 bar. Images were taken 30 s after valve closure.

At 40V, CCGF is clearly observed. This is opposite to the findings in the simulations of Plecis et al, where increase of voltage leads to a shift of the cathodic concentration modes to the CS regime. An explanation for this is that the increased EOF induced pressure enlarges the nanospace height, which in turn allows for higher flow rate. At increased voltages, the relative contribution of the bulk flow becomes more significant. At 60 and 80 V, ACGF occurs. At 100V, small amounts of fluorescein are leaking through the nanospace, indicating the transition towards an AS regime. At 120V, AS is evident: all fluorescein is transferred through the nanospace, though some concentration is still occuring at the anodic side of the valve.

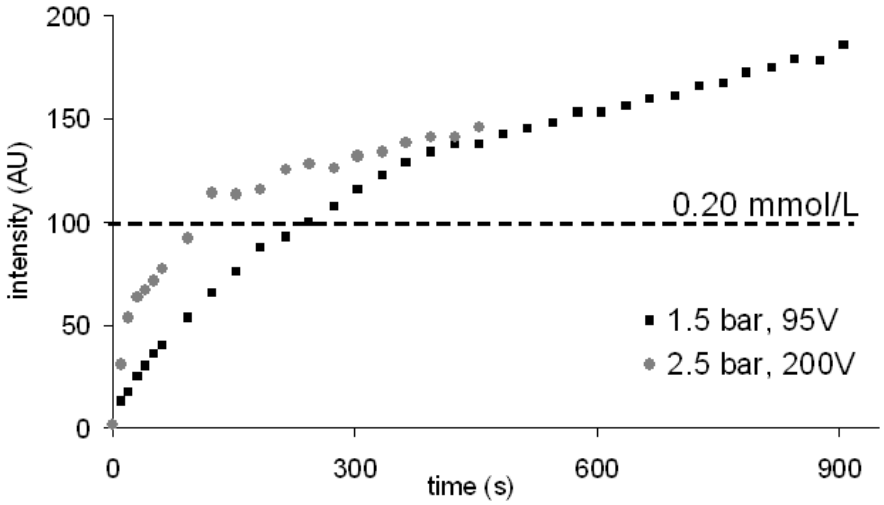

Figure 5. Graph of the increase of fluorescence intensity peak values during focusing of 200 nmol/L fluorescein in 2.0 mmol/L lithium carbonate. The results of two experiments are shown, using 1.5 bar valve pressure and 95 V (squares) and 2.5 bar and 200 V (circles). The dashed line represents the fluorescence intensity corresponding to 0.20 mmol fluorescein, indicating 1000-fold preconcentration.

1000-fold preconcentration and analyte plug release.

We determined preconcentration factors during ACGF focusing of a 200 nmol/L fluorescein solution. Figure 5 shows the development of the fluorescence intensity values in a focused peak. The dashed line corresponds to the intensity measured in a control solution of 0.20 mmol/L fluorescein, indicating the points at which 1000-fold preconcentration is achieved. In a first experiment, valve pressure was 1.5 bar and the external voltage was 95 V. In this experiment, 1000-fold concentration was achieved in about 270 seconds. In a second experiment, a higher valve pressure (2.5 bar) was applied in order to allow higher voltages. We found that at this valve pressure, 200V could be applied to achieve the ACGF regime, which would not be possible with lower valve pressures (at 1.5 bar the inefficient AS regime is dominant for voltages above 100 V, as discussed above). The higher voltage led to more efficient analyte trapping and 1000-fold preconcentration was achieved in only ~100 seconds.

As the depletion zone grows, an increasing amount fluorescein is trapped in the shallow regions alongside the depletion zone and is thus not benefiting the increase of peak intensity. Including a controlled feedback loop to stabilize the size and position of the depletion zone could significantly reduce this effect. While the total fluorescence signal showed linear increase (R^2=0.9965 at 100V and R^2=0.9972 at 200V), the increase in maximum fluorescence intensity slowed down over time. The discrepancy between a constant supply of analyte and a slowing increase in maximum fluorescence intensity can be explained by the observed peak broadening.

Valve opening.

After preconcentration in the ACGF regime, fluorescein could be released by opening the valve (figure 6). A voltage of 200V was applied during valve opening, and valve pressure was 2.5 bar before valve opening. After valve opening, EOF transports the fluorescein zone towards the cathodic reservoir. As the focusing condition is no longer present, sample dispersion takes place, resulting in peak broadening and a decrease of peak concentration. 4 s after valve opening, the peak concentration was decreased about two-fold. Despite sample dispersion after valve opening, sample trapping in the ACGF regime is still highly advantageous as concentration factors can be several orders of magnitude higher.

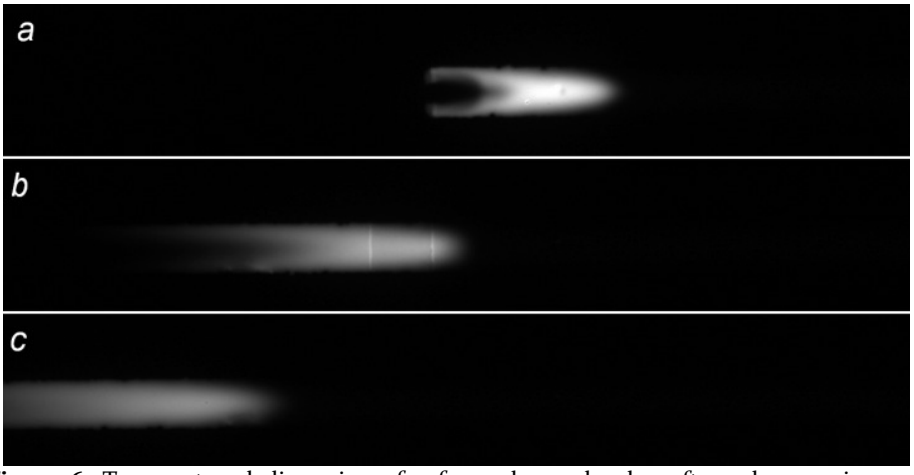

Figure 6. Transport and dispersion of a focused sample plug after valve opening; applied voltage was 200V. a) The concentrated sample plug just before valve opening. b) Sample plug 2 s after valve opening. c) Sample plug 4 s after valve opening.

Conclusions and perspectives

PDMS microvalves have found widespread use and have been instrumental for many successful academic and commercial microfluidic applications. This

research provides evidence that such valves can be used as tunable reversible nanochannels. Measurements of electrical resistance across closed valves indicated the presence of a nanospace with heights in the order of 7 - 55 nm, dependent on the valve pressure. A wide range of concentration polarization regimes could be achieved just by tuning the microvalve pressure, while only requiring a single fluidic channel and a single electrolyte concentration. These regimes were very similar to the regimes predicted in previously published theoretical work. EOF-induced pressure appeared to have a significant effect on the size of the nanospace opening between the valve membrane and the channel walls, as concentration polarization regimes strongly depended on applied voltage. Efficient preconcentration of fluorescein was achieved and could be further improved by increasing both valve pressure and voltage, resulting in 1000-fold preconcentration in 100 s. After valve opening, the concentrated sample plug was transported past the valve, although this was accompanied by some dispersion of the sample plug.

Future studies should further optimize the design of elastomeric valves for nanochannel applications. Possibly a three-state valve can be made, which, dependent on applied pressure, is in open, nanospaced or completely closed state. In our devices, concentration polarization occurred only at relatively low electrolyte concentrations. Perm-selectivity may be improved by increasing the PDMS surface charge, for example using a coating, making the device compatible with a wider range of electrolytes and samples. An important next step is massive parallelization of the valve-based tunable nanochannels.

In biochemical assays that are performed in PDMS devices containing microvalves, our research will find several applications for efficient trapping

and preconcentration of charged components, improving reaction rates and detection limits.

References

1. M. Napoli, J. C. T. Eijkel and S. Pennathur, Lab on a Chip **10** (8), 957-985 (2010).
2. A. Plecis, R. B. Schoch and P. Renaud, Nano Letters **5** (6), 1147-1155 (2005).
3. R. B. Schoch, J. Han and P. Renaud, Reviews of Modern Physics **80** (3), 839 (2008).
4. R. Karnik, C. Duan, K. Castelino, H. Daiguji and A. Majumdar, Nano Letters **7** (3), 547-551 (2007).
5. Z. S. Siwy, Advanced Functional Materials **16** (6), 735-746 (2006).
6. R. Karnik, R. Fan, M. Yue, D. Li, P. Yang and A. Majumdar, Nano Letters **5** (5), 943-948 (2005).
7. Q. Pu, J. Yun, H. Temkin and S. Liu, Nano Letters **4** (6), 1099-1103 (2004).
8. T. A. Zangle, A. Mani and J. G. Santiago, Chemical Society Reviews **39** (3), 1014-1035 (2010).
9. Y.-C. Wang, A. L. Stevens and J. Han, Analytical Chemistry **77** (14), 4293-4299 (2005).
10. S. J. Kim, Y. A. Song and J. Han, Chemical Society Reviews **39** (3), 912-922 (2010).
11. S. M. Kim, M. A. Burns and E. F. Hasselbrink, Analytical Chemistry **78** (14), 4779-4785 (2006).
12. J. Quist, K. G. H. Janssen, P. Vulto, T. Hankemeier and H. J. van der Linden, Analytical Chemistry **83** (20), 7910-7915 (2011).
13. J. Quist, P. Vulto, H. van der Linden and T. Hankemeier, Analytical Chemistry **84** (21), 9065-9071 (2012).
14. L. F. Cheow and J. Han, Analytical Chemistry **83** (18), 7086-7093 (2011).
15. S. Yu, T.-J. Jeon and S. M. Kim, Chemical Engineering Journal **197** (0), 289-294 (2012).
16. S. J. Kim, S. H. Ko, K. H. Kang and J. Han, Nature Nanotechnology **5** (4), 297-301 (2010).
17. A. Plecis, C. m. Nanteuil, A.-M. Haghiri-Gosnet and Y. Chen, Analytical Chemistry **80** (24), 9542-9550 (2008).
18. T. Thorsen, S. J. Maerkl and S. R. Quake, Science **298** (5593), 580-584 (2002).
19. M. A. Unger, H.-P. Chou, T. Thorsen, A. Scherer and S. R. Quake, Science **288** (5463), 113-116 (2000).

20. D. C. Duffy, J. C. McDonald, O. J. A. Schueller and G. M. Whitesides, Analytical Chemistry **70** (23), 4974-4984 (1998).
21. C.-Y. Chen, C.-H. Chen, T.-Y. Tu, C.-M. Lin and A. M. Wo, Lab on a Chip **11** (4), 733-737 (2011).
22. Y.-C. Wang, M. H. Choi and J. Han, Analytical Chemistry **76** (15), 4426-4431 (2004).